Light Metals 2013 *Edited by: Barry Sadler*
TMS (The Minerals, Metals & Materials Society), 2013

Laser Mapping of Carbon Bake Furnaces

Ashley Tews[1], Mike Bosse[1], Robert Zlot[1], Paul Flick[1], Meaghan Noonan[2]

[1]Commonwealth Scientific and Industrial Research Organisation (CSIRO)
Queensland Centre for Advanced Technology; Pullenvale, Queensland, Australia
[2]Pacific Aluminium, Brisbane, Queensland, Australia

Keywords: automation, carbon bake, analysis

Abstract

The flue walls in carbon bake furnaces (CBFs) deform over time under cyclic heating and cooling, leading to difficulties in loading/unloading anodes, and inconsistent anode baking. It is useful to regularly measure the deformations to establish the rate of deterioration and assist in the prediction of flue wall life. Boyne Smelters Limited commissioned a new CBF in 2012. During commissioning, CSIRO utilised its 3D laser scanning technology to map the CBF. A sensor payload consisting of a scanning laser rangefinder sensor connected to a logging and processing PC was suspended from a crane and moved over open pits in a pattern to obtain sufficient coverage of internal pit surfaces, as well as some of the CBF floor and walls. The resulting data is useful for comparing the finished CBF to blueprint plans, and serves as a baseline for future scan comparisons to determine deformations of the flue walls and pit floor.

Introduction

A carbon baking furnace (CBF) consists of interconnected, hollow refractory flue walls through which hot gases are drawn. The heat is conducted through the brick walls to the carbon anodes, improving the anode properties for the electrolysis process. The flue walls deform under this cyclic heating and cooling, leading to difficulties in loading and unloading anodes from the pits, process issues and/or structural instability. Regular maintenance prolongs the working life of the flue walls until replacement is required.

The flue wall condition is monitored to assist with maintenance planning and predicting flue life. Assessments are typically conducted manually and therefore, can be subjective.

Improved assessment systems use physical observations and measurements to calculate a risk score, but time constraints still limit the frequency of assessments and the level of detail captured. The concept of using a more automated approach to obtain three-dimensional (3D) maps of refractory surfaces in the CBF is therefore attractive.

CSIRO has substantial experience with developing 2D and 3D sensing systems [1–3] that are capable of creating data representations that can be used for mapping, navigation or dimension extraction of surfaces such as walls, floors and infrastructure. These systems consist of off-the-shelf hardware configured to provide data to the software that CSIRO has developed. The software integrates the data to produce maps in the form of 3D point clouds, where the accuracy, precision, density, and coverage depend on the sensor motion and technical specifications. Typically, the sensors used are 2D scanning laser rangefinders that provide time-of-flight range measurements to the nearest surface. Moving the sensors around an environment allows for measurements to be gathered from all surfaces observed by the scans of the sensors.

Boyne Smelters Limited (BSL) commissioned a new sixty-six-section, Rio Tinto Alcan AP technology open baking furnace in early 2012. This presented an opportunity for access to a larger number of empty pits than is possible on a fully operating furnace. CSIRO proposed the use of sensing systems to gather 3D data relating to the shape and position of floor and pit surfaces. The project involved using 3D scanners to effectively 'map' the floor, walls and pits in areas of the CBF, with particular focus on the open sections.

Data Acquisition

In this section, the equipment setup and data acquisition steps are described.

Equipment

3D surface mapping equipment is readily available off-the-shelf but mapping can be time-consuming and/or expensive. A common approach is to use surveying equipment statically set up on a tripod at pre-determined locations around the area to be mapped. The sensor rig is then moved to different locations to ensure adequate coverage. This is a highly manual process that can produce accurate

results, and requires qualified operators to use the equipment and process the data. For a CBF layout, placement of surveying equipment would be particularly challenging both due to the geometry of the environment, and the difficulty of situating equipment on floor locations between the pits.

As part of improving mobile robotics applications for industry, the CSIRO team have developed hardware and software systems for 3D mapping using off-the-shelf, relatively inexpensive equipment and in-house technology for processing the data into appropriate representations. For CBF scanning, a prototype sensor rig was developed for data acquisition.

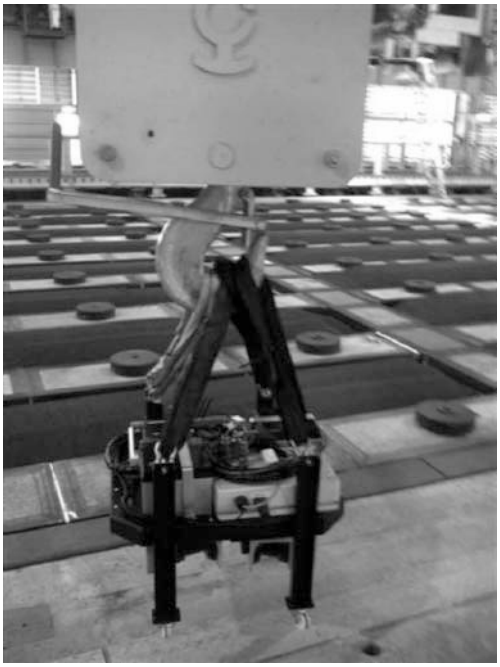

Figure 1: The sensor rig attached to a crane in the CBF. The lidar sensors can be seen under the rig's frame with the control and logging PC, batteries and cabling above it.

The rig, shown in Figures 1, 2, and 3, consists of several scanning laser rangefinder (lidar) sensors and an Inertial Measurement Unit (IMU) connected to a logging and processing PC. The rig was made to be rugged and attached to a crane's hook by standard slings. The crane can then 'trawl' the rig over the areas to be scanned, including descending into the pits if required. The design is intended to enable simple setup and independent operation for acquiring the range data without requiring complex interfaces with existing equipment.

While several laser scanners were mounted on the rig

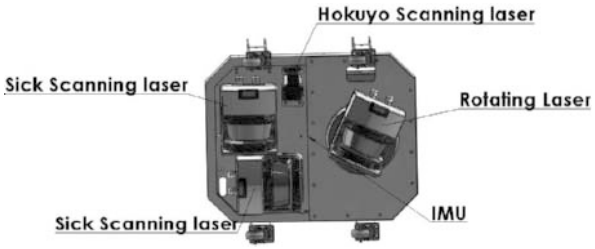

Figure 2: The schematic of the sensor rig, showing the lasers and IMU location.

(Figure 2), only the rotating laser was used for mapping purposes (the others were included to increase coverage and point density, but were later deemed unnecessary). The rotating laser consists of a SICK LMS 291 lidar on a spinning platform. The SICK lidar measures range values in a single plane with a 180° field of view and 1° angular resolution at 75Hz. By spinning the sensor using a rotation motor mounted to its base, the scan plane is no longer fixed, and the resulting configuration results in a hemispherical field of view. Due to radial dispersion, nearby objects will have a higher density of scan points as compared to objects farther away; however, by moving the sensor around the environment, local measurement densities increase over time. The noise level of the range measurements are predominantly determined by the laser hardware (2–3cm for the SICK LMS 291). Through post-processing of the data, better accuracies are possible by averaging over multiple returns where sufficiently high point densities are obtained.

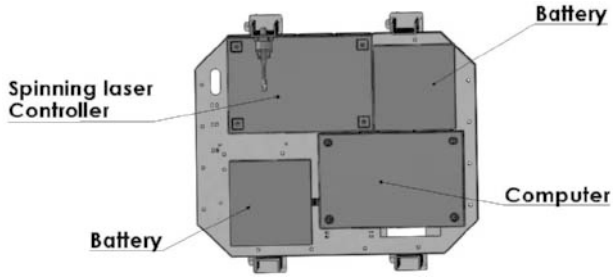

Figure 3: The schematic diagram of the top view of the sensor rig.

In order to generate a globally consistent point cloud model, it is necessary to accurately estimate the trajec-

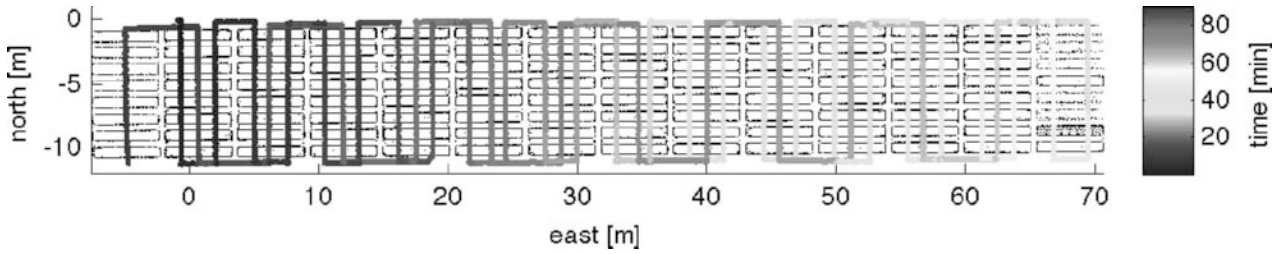

Figure 4: The crane path over sections open pits (black rectangles). The path is coloured by time according to the legend on the right. The entire scanning time for the 14 sections was approximately 90 minutes which was a limitation of maximum crane speed rather than as a requirement of the mapping system.

tory of the sensor payload; that is, the position and orientation of the device at all times. The trajectory is estimated using software developed at CSIRO which uses the relative changes in lidar returns to infer the motion of the payload through the environment [2]. The IMU provides additional rotational rate and translational acceleration measurements which can improve the reliability of the trajectory estimate and ensure that the direction of gravity is known.

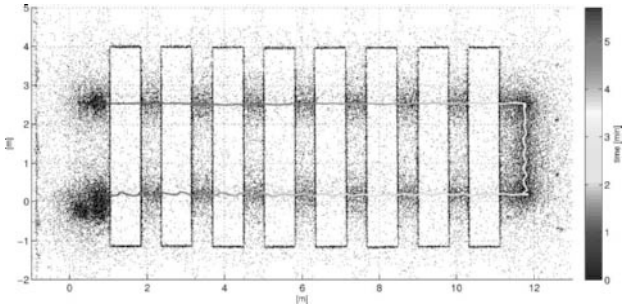

Figure 5: Time-coloured path of the sensor rig over a section during a forward pass. The black dots represent processed scan points. The wobble in the path was the rig swinging under the crane. Note that the effect of the swing has been corrected in the registered points (i.e. the underlying points form straight lines around the pits).

Data Collection

At BSL, one of the CBF cranes was made available for data collection. The sensor rig was suspended from the crane and a series of initialisation tests undertaken prior to the main data gathering exercise. For an initial calibration run, the sensor rig was lowered into a pit.

From the initialisation tests, a crane path was determined over 14 new sections with open pits and then moved opportunistically around covered pits and the CBF to get a general coverage. For most sections of open pits, the crane made three lateral passes (two on the first pass and one on a return run) to allow for adequate coverage. Note that the sensor rig was developed to allow scanning inside the pits by passing over them rather than having to lower the rig into them. The path of the crane over the open pits from one sequence can be seen in Figure 4.

The actual path of the sensor rig from a data sequence collected over the pits of a single section is shown in Figure 5. The colour change on the path represents the time progression from the start (blue) to the end (red). The wobble in the path is the swing after the rig was picked up or changes direction (which is correctly detected by the trajectory estimation software). The rig's trajectory is shown over the processed laser data points seen from an overhead view.

After gathering data from the open pits, the sensor rig was also trawled over other areas of the CBF to allow for supplementary data gathering. The logged data was then processed as discussed in the following section.

Data Representation

Data gathered from scanning is in a raw and unregistered form, and does not constitute a consistent point cloud model until compensation has been made for the payload motion. CSIRO's technology addresses the problem of estimating the sensor trajectory and the environment map concurrently, a problem which is known in the Robotics literature as Simultaneous Localisation and Mapping (SLAM). As the sensor payload moves, features in the environment appear to shift from the scanner's point of view. However, since the environment is assumed to be predominantly static, these apparent motions can

be used to correct for the scanner trajectory. The trajectory corrections are derived from solving a system of constraints including surface patch correspondences, trajectory smoothness, and IMU measurement constraints. Given the globally registered trajectory, the laser range measurements can be projected from the appropriate sensor positions and orientations to produce a consistent point cloud. The point cloud can be saved in a file format for further analysis or visualisation in 3D viewing software. Further analysis is then possible such as extraction of dimensions or surface distortion properties.

The remainder of this section discusses the results from scanning the CBF from a high level overview of the entire CBF down to analysis of a pit, as an example of the potential of the mapping process.

Entire CBF

Figure 6 shows a topdown view of the processed 3D data points over the end of the CBF that contained the open pits. From this high level view, the pits, floor and various infrastructure are clearly identifiable. The density of the data is evident by the solidity of the colours on the furnace features. The area around the open pits is particularly dense since it was the main area to be mapped, and the crane made three passes over most of those pits compared with only a single pass over the rest of the CBF. From this representation, major dimensions of the CBF can be determined.

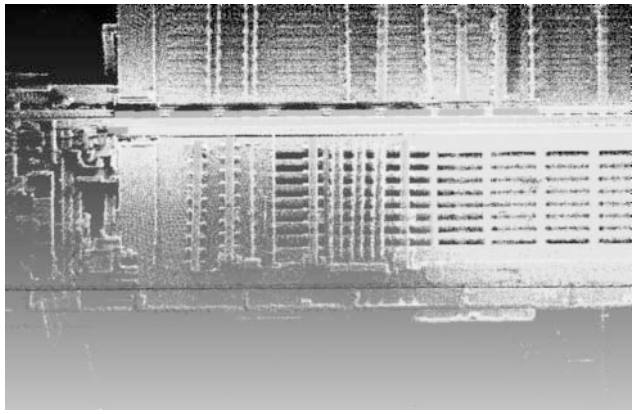

Figure 6: A partial view of the CBF showing the pits in operation at the top of the figure and the empty pits (shown in blue) in the lower right. The colours pertain to height with blues being low and ochres being high. The CBF floor is consistently green indicating its uniform flatness. Firing equipment can been seen in yellow.

Pit Analysis

Since the floors and walls have many scan points to represent them in the data, they may be represented and statistically analysed in a number of ways. For example, the data points on a pit wall can be examined either individually or over small averaged windows. Given the potentially large amount of data (thousands of scan points on a single pit wall), merging points into larger reference windows offers a more appropriate representation.

Given that the open pits have never been used, the walls should be relatively flat and parallel within some arbitrary level of accuracy. This is not an assumption taken by the mapping system as it does not place constraints on the data representation such as flatness or squareness.

Since pit shape and uniformity is of importance for data analysis, the remainder of this section provides an example analysis of an open pit. The analysis method is chosen for ease of demonstration and others may be more useful to the end user.

The figures in this section represent an exploded view of the pit, i.e. the pit has effectively been 'opened' like a box. The pit floor is shown at the bottom of the figure (at approx. x = -7 to -2, y = -6). The colours in each figure show the respective values represented in the legend on their right. Each figure identifies different aspects of the information available from the processed data.

Figure 7 shows the density of scan points falling on the walls and floor. Since the sensor rig passed only over the top of the pit, fewer points fall lower down the pit, evident by the blue values the further down the walls. These values represent the number of scan points falling per 'pixel' where a pixel represents a 10x10 cm cell or window.

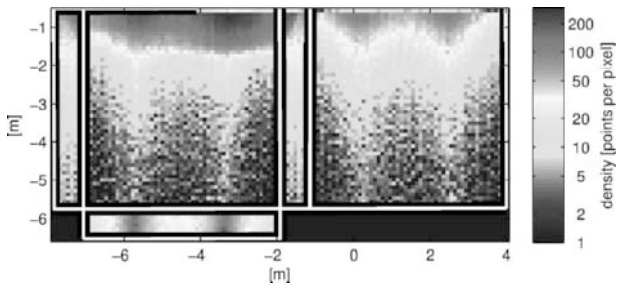

Figure 7: Density of data points falling in 10x10cm grid cells on each surface of a pit. Each surface is shown bounded by a black border with the four walls in the upper part of the figure and the floor at the bottom.

Using the same pixel resolution, an analysis of the

points that fall into each cell can show both the accuracy and precision of the data. Accuracy is determined by the taking the average value of all points in each pixel and comparing their distance to a plane fitted to all data points for that surface (wall or floor). A value of 0 would indicate the average value of all points falls on the plane. In Figure 8 , the accuracy is shown for each cell. Deviations represented by the extreme colours are more prevalent in the lower walls which correlates with the lower point density.

Precision can be considered as the 'spread' of the points around the average value. For example, a cell with an estimated average value of 0 (therefore, accurate) may have a large spread of points around it. The precision value quantifies this spread. Figure 9 shows the precision estimate for each pixel.

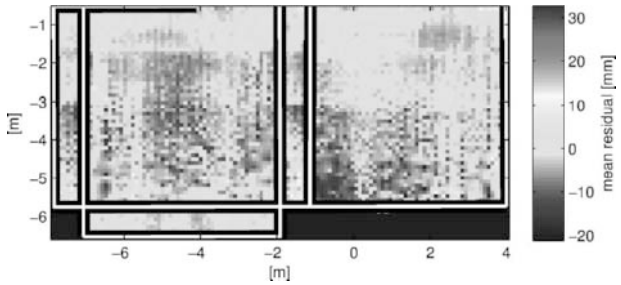

Figure 8: Accuracy analysis calculated using the processed data. Green values represent no deviation and other colours represent indents (redder values) or projections (bluer values). These deviations may be either real or virtual artifacts caused by sensor noise and a sparsity of points in those regions.

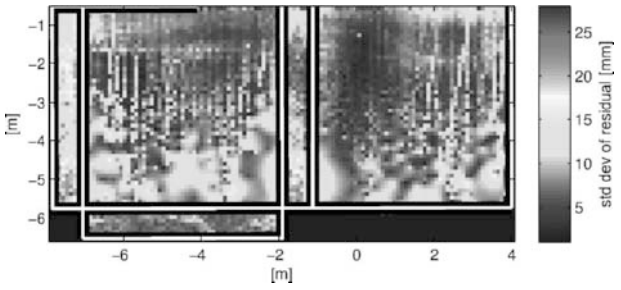

Figure 9: Precision estimate for the processed points. Note that most are within 10 mm.

Statistical Estimations of a Section

The previous analysis provides an indication of the variance and quality of the processed data, assuming the surfaces of the pit are uniformly flat. A general analysis was conducted of the processed data to determine the outer dimensions of each pit including the variance on these measurements. The measurements were based on computing the average distance between planes fitted to opposing surfaces using the processed data as a guide to plane-placement. The calculated variance is estimated 'noise' or dispersion of the points used in the calculation. The resulting estimations were compared against blueprint plan dimensions as well as physical measurements taken by Pacific Aluminium staff.

Variations are differences between estimated measurements and the actual dimension and can be due to: the walls not being built exactly to plans, walls not being perfectly planar, and/or sensor noise. Tables 1, 2, and 3 below show the dimensions for length, width and height of all eight pits in a single section. For the length and width, the measurements were made between opposing surfaces. For the depth, the location of the top of the pit was estimated and depth analyses were based on this offset. Hence, the errors may include a small constant bias in one direction.

If the pits of the section were made to the dimensions provided (5100mm length, 795mm width, and 5710mm depth), then the errors from our estimation of the dimensions were: length 12-30 mm, width 0-5mm width, and depth 30-50mm. Note that these were estimates taken from further processing the data and do not represent the accuracy of the data points, only of the manner in which these dimensions were calculated.

Summary

Lidar-based sensing systems have the potential to provide data-rich records of refractory condition which will likely assist maintenance planning and flue life prediction. A key opportunity existed with the newly constructed CBF at BSL to gather baseline data of pit surfaces and the CBF floor.

During data gathering, the entire CBF was surface scanned with 14 sections of open pits allowing for internal scanning. The time for scanning an open section using the prototype sensor rig was less than six minutes, though this was due to the crane speed rather than a data gathering requirement. The entire CBF was scanned in approximately 90 minutes. This is substantially faster and more automated than existing methods considering the sensor

Table 1: Estimated pit widths and variances. Ideal actual pit width = 795mm.

Pit:	1	2	3	4	5	6	7	8
Mean width (mm):	795.4	794.87	798.03	794.67	795.5	796.64	800.43	798.29
Stddev (mm):	9.47	9.82	9.57	11.14	8.4	9.33	11.29	12.385

Table 2: Estimated pit lengths and variances. Ideal actual pit length = 5100mm.

Pit:	1	2	3	4	5	6	7	8
Mean Length (mm):	5130.1	5122.1	5129.5	5117.4	5115.7	5127.5	5122.7	5124.5
Stddev (mm):	15.2	16.96	11.89	18.79	13.99	12.89	12.58	14.97

Table 3: Estimated pit depths and variances. Ideal actual pit depth: approx 5710mm.

Pit:	1	2	3	4	5	6	7	8
Mean Depth (mm):	5740.7	5745	5751.9	5755.2	5762.1	5747.6	5749.5	5743.7
Stddev (mm):	8.8717	8.5198	9.1178	8.0469	7.8063	8.4923	7.0358	7.7731

payload only needed to be turned on and picked up by the crane with no other setup.

In future iterations of the project, the prototype sensor rig will be redesigned to be more ergonomic or may be replaced by a permanent sensor system mounted to the crane. The data can be periodically processed through the 3D mapping system and a client-based application can analyse it to create reports on pit distortions. Automating this process has the advantages over the current human-derived methods by being more consistent and less prone to human measurement errors, and alleviates the manual effort required.

References

[1] M. Bosse and R. Zlot, "Map matching and data association for large-scale 2D laser scan-based SLAM," *International Journal of Robotics Research*, vol. 27, no. 6, pp. 667–692, June 2008.

[2] ——, "Continuous 3D scan-matching with a spinning 2D laser," in *IEEE International Conference on Robotics and Automation*, May 2009, pp. 4312–4319.

[3] R. Zlot and M. Bosse, "Efficient large-scale 3D mobile mapping and surface reconstruction of an underground mine," in *Proceedings of the International Conference on Field and Service Robotics*, 2012.